Resilient Event-Triggered Terminal Sliding Mode Control Design for a Robot Manipulator

Mobin Saeedi, Jafar Zarei, *Member, IEEE,* Mehrdad Saif, *Senior Member, IEEE,* Declan Shanahan, Allahyar Montazeri, *Member, IEEE,*

Abstract—A novel non-singular terminal sliding mode controller (NTSMC) has been developed for the purpose of tracking and stabilizing tasks in uncertain electro-hydraulic robot manipulators. It is supposed that the controller communicates with the robot through a network that is vulnerable to cyber-attacks. To reduce the communication burden on the network layer and achieve resilience against cyber-attacks, an event-based strategy is employed. For this purpose, the event-triggering rule is derived so that the Zeno-free behavior is guaranteed. Then, based on the cyber-attack characteristics, i.e., frequency and duration of the attacks, the resilient behavior of the proposed scheme in the presence of denial of service attacks, unmodelled dynamics, and external disturbance are analyzed. Moreover, to capture the nonlinear nature of the robot an experimentally validated analytical model of an uncertain 7-DoF manipulator with a hydraulic model of the joints and actuators, namely, Brokk-Hydrolek, is employed. Finally, the merits of the proposed methodology in terms of resiliency, robustness, and preservation of the communication resources are validated, and the results are compared to the state-of-the-art approaches based on the ρ index criterion.

Note to Practitioners—The aim of this study is to address the problem of network-based control of robotic manipulators. Currently, the majority of manufacturers and companies utilize programmable logic controllers to drive dynamic manipulators. These systems commonly use the network layer to collect measurement data and/or transmit control commands. Therefore, they are always susceptible to cyber-attacks that can have catastrophic consequences. Furthermore, they should comply with network restrictions, such as limited bandwidth, in order to achieve the desired performance. Therefore, due to the collaborative behavior of robot manipulators in industries, it is vital for engineers and practitioners to be assured of achieving desired performance in the presence of these threats and limitations. As a first step in this paper to deal with these issues, a 7-DoF robotic manipulator model is mathematically formulated and experimentally validated. Then, a controller design procedure that guarantees the desired performance in spite of model uncertainties, denial-of-service cyber-attacks, and network restrictions is derived. Additionally, a clear relation between cyber-attack characteristics and designed parameters is defined while resilient behavior is maintained. Note that the proposed approach can be applied to a wide range of network-based nonlinear dynamic systems.

M. Saeedi is with the Department of Electrical and Electronics Engineering, Shiraz University of Technology, Shiraz, Iran (email: m.saeedi@sutech.ac.ir).

J. Zarei is with the Department of Electrical and Electronics Engineering, Shiraz University of Technology, Shiraz, Iran, and also with the Department of Electrical and Computer Engineering, Windsor University, ON N9B 3P4, Canada. (e-mail: zarei@sutech.ac.ir, jzarei@uwindsor.ca).

Declan Shanaban and Allahyar Montazeri are with the Engineering Department of Lancaster University, Gillow Avenue, Lancaster, England, LA14YW. (e-mail: d.shanahan1@lancaster.ac.uk, a.montazeri@lancaster.ac.uk).

Index Terms—Robot manipulator, robust control, denial-of-service (DoS) attack, event-triggered control, terminal sliding mode.

I. INTRODUCTION

IN recent years, dexterous robotic manipulators have played an important role in a wide range of services and industries, such as healthcare and manufacturing systems. They also find key applications in harsh and hazardous environments such as nuclear-decommissioning tasks, where remotely operated manipulators are a great asset to reduce the exposure of workers to radioactive environments [1]–[5]. Most common actuators that are utilized in robotic manipulators can be categorized into three main classes, that are, pneumatic, electro-hydraulic, and servo motors. The ability of electro-hydraulic actuators to produce significant torque despite their small size, have attracted most engineers and researchers to develop electro-hydraulic robotic manipulators (EHRM) [6]. Despite the complexity, inherent nonlinear characteristic, coupling dynamics, and time-varying parameters, EHRMs have received a lot of interest in both academia and industry [7]. The task execution performance of the manipulator under such conditions is extremely degraded in terms of accuracy and precision, especially when the robot needs to operate autonomously and independently from the operator [8].

Different control approaches, such as intelligent control methodologies [10], [11], and nonlinear model-based control techniques [12] are developed to control different types of EHRMs. Although intelligent control schemes such as neural network (NN) based controllers are suitable to avoid ambiguity in the mathematical modeling of EHRMs, these approaches suffer from a high computational burden [13]. This issue becomes vital when communication networks are employed to transmit data in closed-loop systems. However, the advent of the internet of things and associated digital communication, has increased the utilization of the networked manipulators in a wide area such as humans-assisted manipulators in the surgical field [11], and remotely operated manipulators in hazardous environments [14]. In the industrial environment, this requires the involvement of the robotic manipulators as an integrated part of the cyber-physical systems (CPSs), and hence networks are becoming an integrated element of the manipulator's control strategies [15], [16]. Due to the hierarchy of different interactive networked elements such as sensors, controllers, and actuators, cyber-physical systems, and their challenges become one of the most important research fronts in recent years [17].
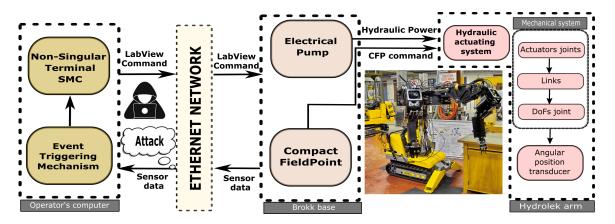
Fig. 1. The overall scheme of Brokk-Hydrolek 7-DoF manipulator under control of event-triggered non-singular terminal SMC in presence of cyber-attacks that ruin measuring data [9].

On the other hand, according to the reported performance of EHRMs' under different kinds of controllers, nonlinear approaches demonstrate prominent stability-guaranteed performance in position tracking, and regulation tasks [13], [18]. Although a wide range of these techniques such as back-stepping methods [19], model predictive control approaches [20], and adaptive procedures [21] have been utilized to control robotic manipulators, one of the most effective methods to overcome the uncertainties and unknown dynamics in the system is the sliding mode controller (SMC) schemes [18]. Due to the robust performance and its simplicity in practical applications, the SMC has been applied in a wide variety of dynamic systems [7]. Although traditional SMC introduced so many advantages as a robust controller, it suffers from drawbacks such as the disability to guarantee convergence in a predefined time. Therefore, to overcome these drawbacks, this methodology is being developed. Accordingly, to achieve finite-time convergence, and enhance the convergence characteristic, terminal SMC (TSMC), fast terminal SMC (FTSMC), and non-singular FTSMC (NFTSMC) were proposed [22], [23]. Meanwhile, a combination of these well-established nonlinear control schemes with intelligent theories such as NN, and T-S Fuzzy introduced a new research front [24]. It should be noted that providing a criterion to compare the performance of robotic manipulators under different control algorithms is always a challenging issue. Thus, some indexes such as ρ indicator [18], [25], maximum, average, and standard deviation of tracking error denoted as M_e, μ, and δ [26] were introduced.

All CPSs including networked EHRMs, are always exposed to two main concerns, i.e., limitations in communication resources, and security [17], [27], [28]. Event-based control strategies are one of the most effective approaches to reducing communication and computation burden, and increasing resilience against cyber-attacks and network packet-dropout [29], [30]. Event-based terminologies can be roughly divided into two main categories based on the triggering rule and the kind of underlying dynamic system. In other words, the dynamic system can be represented as a linear or nonlinear model while static or dynamic triggering rules can be employed to update the control action [31]. When the non-linearity, and ambiguity of the mathematical model of the dynamic systems are increased, more computational analysis is required to guarantee the stability, and achieve Zeno-free behavior of the closed-loop system. Therefore, applying the event-based schemes to the EHRMs' model emerges a new research area due to the inherent complexity of the nonlinear model of EHRMs. The resilience behavior of the designed controllers is always a challenging issue, especially when networked EHRM's tasks are safety-related issues in critical applications, such as nuclear decommissioning tasks where any malfunction due to the cyber-attack would result in catastrophic effects. Therefore, robust approaches are exploited to design resilient controls to address these issues as well as existing uncertainties in the network [32]. For example, in [33] the cyber-actuator attack is studied and a robust SMC with a linear sliding surface is designed for the linear uncertain dynamic system. Dissipative-based SMC in the presence of a Denial-of-Service (DoS) attack is proposed in [27] where a linear sliding surface for the general form of the linear dynamic system is designed. Meanwhile, some studies employed intelligent control strategies to address the effect of DoS attacks. For example, an adaptive fuzzy controller is designed for uncertain nonlinear dynamic systems in presence of a DoS attack [34]. A resilient control methodology can be viewed from two perspectives. In one approach, the controller design and the closed-loop stability analysis are performed in the presence of attack detectors or compromised-data estimators [35]–[37].All data-driven approaches that propose the attack detection mechanisms such as data-watermarking, and queue model analysis are classified in this category of resilient control methodologies [38]–[41]. On the other hand, some approaches does not utilize any detection mechanism, rather than they analyze the resilient behavior of the designed controller based on the attacks' characteristic such as frequency and duration [42]–[44]. This paper investigates the resilient control design based on the second viewpoint.

The robotic manipulator chosen for this study is a bespoke dual-arm 7-DoF hydraulically actuated mobile manipulator, named Brokk-Hydrolek which is developed based on experimental results in the laboratory. Several efforts have been made to derive a dynamic model and estimate the parameters of the robot by collecting experimental data from the robot [9], [45]. For example, in [46], [47] a multi-objective genetic algorithm is proposed

to address the non-convexity of the performance index used for the parameter estimation while a state-dependent parameter model is developed in [48] to compensate for the dead-zone non-linearity in the controller design. As reported in [7], the use of model-based control design techniques such as sliding mode control is promising to handle the nonlinearities in such a hydraulically actuated manipulator. For this purpose, a 2-DoF analytical model of the manipulator is derived and verified using experimental results. Here, the effect of other links is considered as the dynamic uncertainty in the controller design, and the results are verified on the full 7-DoF robotic model developed in [9].

Motivated by these challanges, three main issues should be tackled while the control of networked uncertain EHRM is our concern, namely, robustness, resiliency, and limitation in the communication resources. Therefore, in this study, an event-triggered non-singular terminal SMC is developed for a networked 7-DoF uncertain EHRM in the presence of a malicious DoS attack. The conceptual framework of the problem is illustrated in Fig. 1. The Lyapunov theory is applied to prove the stability of the proposed CPS under cyber attacks. The novelty and core of this study can be summarized as follows:

1) Unlike the proposed methods in [49], [50], this work presents an event-based non-singular TSMC to establish finite-time convergence, robust and resilient performance, and decrease the communication burden in the network layer. Some conservative assumptions such as fixed-bounded uncertainties, and fixed control input direction during inter triggering time are not imposed, which outperform this study compared to state-of-the-art works such as [51]–[55] that propose event-based terminologies for a general form of nonlinear dynamic systems.

2) The proposed approach is evaluated on a novel experimentally validated nonlinear analytical model of the Brokk-Hydrolek manipulator in the presence of uncertainties and benchmarked against other methods proposed in the literature to extend the work to networked hydraulic manipulators.

3) To the best of our knowledge, the resilience behavior of the networked EHRMS under robust controllers has not been considered in recent studies. Accordingly, in current work, the resiliency of the proposed scheme in the presence of DoS attacks is investigated, and explicit relations between cyber-attack characteristics, i.e., frequency and duration, and design parameters are derived.

4) The superiority of the presented methodology to the prior works is validated based on the ρ index which is a common criterion to show the ability of the proposed technique. The reported comparative results illustrate the better robust, and resilient performance while the fewer communication resources are used.

The remainder of this article is organized as follows. The analytical dynamic model of the aforementioned 7-DoF robotic manipulator is proposed in Section II. The controller design methodology is described in Section III. This is followed by the experimental results in Section IV,

and finally, the paper is concluded in Section V.

A. Notation

In order to have a clear formulation of the problem, the following notations are used in this study. $\mathbb{R}$ represents the set of real numbers and $\mathbb{R}_0$ defines the set of real numbers greater than zero. $\mathbb{N}$ defines the set of natural numbers and $\mathbb{N}_0$ denotes the set of natural number including zero, i.e., $\mathbb{N}_0 = \{\mathbb{N} \bigcup \{0\}\}$. Let A, B, C be three sets, $C = A \backslash B$ represents the complimentary set of A and B such that $A = C \bigcup B$. The transpose of matrix M, is defined as M^T. The matrix norm $\| . \|$ defines the spectral norm of the matrix and for a given vector $V \in \mathbb{R}^{n \times 1}$, $\| . \|$ represents the Euclidean norm. $y = diag(x) \in \mathbb{R}^{n \times n}$ expresses diagonal representation of the vector $x \in \mathbb{R}^n$.

II. THE DYNAMIC MODEL OF THE 7-DOF MANIPULATOR

A. Model Description

The dynamic model of the 7-DoF Brokk-Hydrolek manipulator expresses the interactions between the mechanical, hydraulic, and electrical components and as illustrated in Fig. 1, it can be decomposed into several sub-systems. Each joint of the manipulator is equipped with a rotary potentiometer as the feedback sensor, determining the joint angle for the controller. Joints are actuated through the hydraulic pistons that are powered by the hydraulic pumps. The hydraulic fluid passes through a four-way directional spool valve which is operated by two solenoid valves available for each joint as depicted in Fig. 2. The applied voltage commands, V_{amp_a} and V_{amp_b} are converted into coil currents, I_{coil_a} and I_{coil_b} respectively, and energize the solenoid valves according to

$$I_{coil_H} = \begin{cases} I_{\min} & if \ V_{amp} = 0V \\ V_{amp_H} \frac{I_{\max} - I_{\min}}{10} + I_{\min} & if \ 0 < V_{amp} < 10V \\ I_{\max} & if \ V_{amp} \geq 10V \end{cases} ,$$ (1)

where H is either a or b. According to the Newton's law, the dynamic behavior of the plunger actuated by the solenoid valves can be represented as

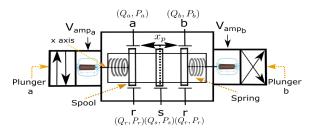Fig. 2. The schematic diagram of a 4-way solenoid valve.

$$F_H = m_{pl} \ddot{x}_{pl} + \lambda_{pl} \dot{x}_{pl} + k_{pl} x_{pl},$$ (2)

where x_{pl} defines the stroke of the plunger. λ_{pl}, k_{pl} are the stiffness and damping coefficients of the plunger, respectively and m_{pl} specifies mass of the plunger. F_H is the solenoid force that is generated on the plunger. The relationship between the plunger displacement and

hydraulic flow rates as well as the hydraulic pressures at the four-way valve's input/output ports can be written as

$$Q_a = \begin{cases} C_q A(x) \, sgn(P_s - P_a) \sqrt{\frac{(2|P_s - P_a|)}{\rho}} & 0 < x < w \\ C_q A_{max} \, sgn(P_s - P_a) \sqrt{\frac{(2|P_s - P_a|)}{\rho}} & x \geq w \end{cases},$$
(3)

and,

$$Q_b = \begin{cases} C_q A(x) \, sgn(P_b - P_r) \sqrt{\frac{(2|P_b - P_r|)}{\rho}} & 0 < x < w \\ C_q A_{max} \, sgn(P_b - P_r) \sqrt{\frac{(2|P_b - P_r|)}{\rho}} & x \geq w \end{cases},$$
(4)

where C_q is the constant coefficient of the valve, w is the maximum valve traveling distance in its sleeve. P_a, P_b, P_s and P_r are the pressure at ports a, b, s and r, respectively. Note that P_s, and P_r are supply and reservoir/tank pressures, respectively. $A(x)$ defines the restrictor area and A_{max} is the $\max\{A(x)|\, 0 < x \leq w\}$. Looking at Fig. 2 along with (3), the dynamic of piston can be written as

$$m\ddot{x}_p + \lambda \dot{x}_p + k x_p = (A_a P_a - A_b P_b) - F, \quad (5)$$

where m, λ, and k are the mass, damper coefficient, and spring stiffness of the piston, respectively. The force F denotes any other force acting on the piston. The areas of the sides a and b of the piston are represented by A_a, A_b, and P_a, P_b are the pressures in chambers a and b of the cylinder. According to the virtual work, the joint torque and the piston force are related according to

$$\tau = \frac{dx_p}{dq} F. \quad (6)$$

The dynamic model of the mechanical part, i.e., manipulator dynamic, can be derived using Newton-Euler method as

$$M(q)\ddot{q} + C(q,\dot{q})\dot{q} + G(q) + F(q,\dot{q}) + D(q,\dot{q}) = \tau, \quad (7)$$

where $M(q) \in \mathbb{R}^{n \times n}$ is the robot mass matrix, $q \in \mathbb{R}^{n \times 1}$ and its derivatives are vectors of joint angles and their derivatives respectively. $G(q) \in \mathbb{R}^{n \times 1}$ is the gravity vector torque, $C(q,\dot{q}) \in \mathbb{R}^{n \times n}$ is related to the Coriolis term and is a matrix of velocity-dependent terms, $F(q,\dot{q}) \in \mathbb{R}^{n \times 1}$ represents the friction dynamic, $D(q,\dot{q}) \in \mathbb{R}^{n \times n}$ is the matrix of unknown disturbance terms, and finally $\tau \in \mathbb{R}^{n \times 1}$ is a vector of input torques.

B. Problem formulation

In this section, the analytical model of the 7-DoF manipulator following the previous equations is derived. The proposed model provides a basis for the next section in which the controller design procedure is developed. By rewriting the manipulator's dynamic (7) as

$$\ddot{q} = M^{-1}(q)(\tau - C(q,\dot{q})\dot{q} - G(q) - F(q,\dot{q}) - D(q,\dot{q})), \quad (8)$$

and omitting the dynamic of piston for simplicity, (5) is reduced to

$$F = (A_a P_a - A_b P_b). \quad (9)$$

Using the linearized model for the flow equation yield

$$Q_\mu = k_q x_\nu + k_p \Delta P_\mu, \quad (10)$$

where ΔP_μ is the pressure drop at the nominal operating pressure, μ is either a or b, and Q_μ represents the flow rate, i.e., Q_a or Q_b according to Fig. 2. k_p is the pressure-flow coefficient, k_q is the flow gain, and x_ν represents the valve displacement. Flow dynamic (10) can be combined with the cylinder flow equation by neglecting the compressibility as

$$A_\mu \dot{x}_p = k_{q_\mu} x_\nu + k_p \Delta P_\mu. \quad (11)$$

Assuming that the return pressure is P_{a_0} and P_{b_0}, $F = 0$ in (9), and having the equality $P_{a_0} + P_{b_0} = P_s$, yields

$$P_{a_0} = \frac{A_b P_s}{A_a + A_b} \quad (12a)$$

$$P_{b_0} = \frac{A_a P_s}{A_a + A_b}. \quad (12b)$$

By considering $\Delta P_a = P_{a_0} - P_a$, $\Delta P_b = P_{b_0} - P_b$, (11), and (12), one can obtain:

$$P_a = \frac{A_b P_s}{A_a + A_b} + \frac{1}{k_p}(A_a \dot{x}_p - k_{q_a} x_\nu) \quad (13a)$$

$$P_b = \frac{A_a P_s}{A_a + A_b} - \frac{1}{k_p}(A_b \dot{x}_p - k_{q_b} x_\nu). \quad (13b)$$

Now, considering the geometry of each joint, the relationship between the rate of change of link displacement and rotation angle of the joint can be written as

$$\frac{dx_{p_i}}{dq_i} = \frac{l_{base_i} l_{link_i} \sin(q_i + q_{a_i})}{\sqrt{l_{base_i}^2 - 2\cos(q_i + q_{a_i}) l_{base_i} l_{link_i} + l_{link_i}^2}}, \quad (14)$$

where i represents joint number, q_{a_i} is a constant offset derived from geometrical representation of each joint, and l_{base_i}, l_{link_i} are manipulator's constant parameters. By combining (13), (14), and (9) the force generated inside each joint can be expressed as

$$F_i = \frac{A_a^2 + A_b^2}{k_{p_i}} \frac{dx_{p_i}}{dq_i} \dot{q}_i - \frac{A_a k_{q_{a_i}} + A_b k_{q_{b_i}}}{k_{p_i}} x_{\nu i}. \quad (15)$$

Therefore, the dynamic equation (8) by taking the hydraulic equation into account can be represented as

$$\ddot{q} = M^{-1}(q)(\Phi(q,\dot{q}) + H(q)x_\nu - C(q,\dot{q})\dot{q} \\ -G(q) - F(q,\dot{q}) - D(q,\dot{q})), \quad (16)$$

where $\Phi_i(q,\dot{q}) = \frac{A_a^2 + A_b^2}{k_{p_i}} \frac{[l_{base_i} l_{link_i} \sin(q_i + q_{a_i})]^2}{l_{base_i}^2 - 2\cos(q_i + q_{a_i}) l_{base_i} l_{link_i} + l_{link_i}^2} \dot{q}_i$, $\Phi(q,\dot{q}) = [\Phi_1(q,\dot{q}), ..., \Phi_n(q,\dot{q})]^T$, $H_i(q) = -\frac{l_{base_i} l_{link_i} \sin(q_i + q_{a_i})(A_a k_{q_{a_i}} + A_b k_{q_{b_i}})}{k_{p_i} \sqrt{l_{base_i}^2 - 2\cos(q_i + q_{a_i}) l_{base_i} l_{link_i} + l_{link_i}^2}}$, $H(q) = diag\{H_1(q), ..., H_n(q)\}$. In this case, the dynamic equation (16) can be rewritten in the state space form as

$$\dot{x}_1 = x_2(t) \\ \dot{x}_2 = M^{-1}(x_1(t))\{-\Gamma(x(t)) - D(x(t)) + H(x_1(t))u(t)\}, \quad (17)$$

where $x(t) = [x_1(t), x_2(t)] \in \mathbb{R}^{2n}$, $x_1(t) = q \in \mathbb{R}^n$, $x_2(t) = \dot{q} \in \mathbb{R}^n$ are the state variables, $\Gamma(x(t)) = -\Phi(x(t)) + C(x(t))x_2 + G(x_1) + F(x(t))$, that satisfy Assumption 1, and $u(t) = x_\nu \in \mathbb{R}^n$ is the control input. Moreover, $D(x(t))$ refers to the whole uncertain dynamics including the uncertain friction force, uncertain gravitational torque, and unmodeled dynamic in (8), that satisfy Assumption 2.

Assumption 1: $\Gamma(x(t))$ is Lipchitz on compact set $\Omega \in \mathbb{R}^{2n}$, and satisfies the following constraint,

$$\|\Gamma(x(t)) - \Gamma(x(t^*))\| \le L_0 \|x(t) - x(t^*)\|, \qquad (18)$$

where $L_0 \in \mathbb{R}_0$.

Assumption 2: The uncertain term $D(x(t))$ satisfies following inequality,

$$\|D(x(t))\| \le b_0 + b_1 \|x(t)\|, \qquad (19)$$

where b_0, and $b_1 \in \mathbb{R}_0$.

Remark 1: Note that $D(x(t))$ is a lump sum definition of different parts of the manipulator dynamic including parametric and non-parametric uncerainties.

Assumption 3: First, and second time derivatives of desired states' trajectories are supposed to be known, and bounded.

Assumption 4: The robot mass matrix $M(x_1(t))$, satisfies following constraint for any arbitrary $x_1(t)$,

$$\underline{M}x_1(t)^T x_1(t) \le x_1(t)^T M(x_1(t))x_1(t) \le \bar{M}x_1(t)^T x_1(t), \qquad (20)$$

where $\bar{M}$, and $\underline{M}$ are positive constants.

III. CONTROLLER DESIGN

In this section an event-based terminal SMC in the presence of a DoS attack for the general form of a 7-DoF manipulator is proposed. In subsection III-A, the preliminaries and DoS attack formulation is described. Then, in subsection III-B the controller design methodology is formulated. Admissibility of the proposed event-based controller is investigated in subsection III-C. Finally, in subsection III-D the resilience behavior of the proposed scheme is presented.

A. Denial-of-Service attack formulation

The goal of the DoS attack is to make interruptions in sending commands toward the physical system or making disruptions in receiving sensors and measurement data. The overall scheme of the closed-loop system is shown in Fig. 1. Before designing a resilient control methodology, it is required to formulate the cyber-attack. Moreover, time instances in which a cyber-attack is activated during any arbitrary time interval $t \in \begin{bmatrix} \tau & t \end{bmatrix}$ where $t > \tau \in \mathbb{R}_0$ is defined as

$$\mathcal{D}(\tau, t) = \underset{n \in \mathbb{N}_0}{\cup} \{H_n \cap [\tau, t)\}, \qquad (21)$$

where $H_n := [h_n, h_n + \tau_n)$, $n \in \mathbb{N}_0$, and $h_n, \tau_n \in \mathbb{R}_0$ are the cyber-attack activation time instance and its duration respectively as illustrated in Fig. 3. $A(\tau, t)$ is the complement of $\mathcal{D}(\tau, t)$ and expresses the time duration in which the attacks are deactivated as follows

$$A(\tau, t) = [\tau, t) \setminus \mathcal{D}(\tau, t). \qquad (22)$$

Without loss of generality, well-known assumptions about the duration and frequency property of DoS attack are represented as follows [54].

Assumption 5: There exists $n_0, \tau_0 \in \mathbb{R}_0$ such that the following inequality holds [43],

$$n(\tau, t) \le n_0 + \frac{t - \tau}{\tau_0}, \qquad (23)$$
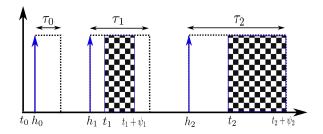

Fig. 3. An example of DoS attacks activation. τ_i, $i \in N_0$ represents duration of DoS attack, i.e. $H_0 = [h_0, h_0 + \tau_0)$, $H_1 = [h_1, h_1 + \tau_1)$, $\mathcal{D}[0, h_1) = [h_0, h_0 + \tau_0)$, and $n[0, h_2) = 2$.

where $n(\tau, t)$ represents the number of cyber-attack occurrence in the time interval $[\tau, t)$ for all $\tau, t \in \mathbb{R}_0$ and $t > \tau$.

Assumption 6: There exists $\nu, \kappa \in \mathbb{R}_0$ such that following inequality holds [43],

$$\mathcal{D}(\tau, t) \le \kappa + \frac{t - \tau}{\nu}, \qquad (24)$$

where $\mathcal{D}(\tau, t)$ represents the cyber-attack duration in the time interval $[\tau, t)$ for all $\tau, t \in \mathbb{R}_0$ and $t > \tau$.

Remark 2: Two main viewpoints can be considered to model the DoS attacks' activation patterns, i.e., stochastic, and deterministic [35], [43]. This work considers the deterministic model of DoS attack while there is no conservatism assumption on the activation pattern of the cyber-attacks.

B. Controller design methodology

In this section an event-based terminal SMC scheme is proposed. To achieve the control objective, in the first step, the sliding surface should be defined. Consider the following non-singular terminal sliding manifold

$$S(t) = \alpha_1 e(t) + \alpha_2 \dot{e}(t)^{p/q}, \qquad (25)$$

where $e(t) = x_1(t) - x_d(t) \in \mathbb{R}^n$ is the tracking error and $x_d(t) \in \mathbb{R}^n$ is the desired state, $\alpha_1, \alpha_2 \in \mathbb{R}_0$ are positive constants, and $p, q \in \{2k + 1 | k \in \mathbb{N}_0\}$ are odd constants that satisfy the inequality $1 < p/q < 2$. The first derivative of (25) with respect to time yields

$$\dot{S}(t) = \alpha_1 \dot{e}(t) + \alpha_2 \frac{p}{q} \dot{e}(t)_d^{p/q-1} \ddot{e}(t), \qquad (26)$$

where $\dot{e}(t)_d^{p/q-1} = diag(\dot{e}(t)^{p/q-1})$. As discussed in the Introduction section, to reduce the communication load, and increase the robustness against the packet-drop out and cyber-attack, an event-based controller is considered as an alternative approach to time-based triggering methodology. Assume t^i, $i \in \mathbb{N}_0$ represents the time instances through which the states are updated and the controller scans the input data. Hence, the event-triggering error for $t \in [t^i, t^{i+1})$ is expressed as

$$E(t) = x(t) - x(t^i). \qquad (27)$$

Lemma 1: In the triggering time duration, i.e. $t \in [t^i, t^{i+1})$, $i \in \mathbb{N}_0$ the region Ξ in which $Sign(S(t^i)) \ne Sign(S(t))$ is the closed region.

Proof. Please see the Appendix for the complete proof.

Lemma 2: In the triggering time duration, i.e. $t \in [t^i, t^{i+1}), i \in \mathbb{N}_0$, $\left\| \dot{e}(t)^{2-p/q} - \dot{e}(t^i)^{2-p/q} \right\|$ is bounded as

$$\left\| \dot{e}(t)^{2-p/q} - \dot{e}(t^i)^{2-p/q} \right\| \leq \prod, \tag{28}$$

where $\prod = \max\{1, (k\frac{\|e(0)\|}{\bar{\Delta}} + \|\dot{x}_d(t)\| + \xi)^{2-p/q} + \|\dot{x}_d(t)\|^{2-p/q}\}$.

Proof. Please see the Appendix for the complete proof.

Assumption 7: Variation of $M(x_1(t))$ in the time interval $t \in [t^i, t^{i+1}), i \in \mathbb{N}_0$ is negligible [55].

Theorem 1: Consider the uncertain manipulator dynamic (17), under the event-triggering rule (30) in the presence of DoS attack, the control effort (29) guarantees the finite-time ultimately globally bounded (UGB) closed-loop response

$$u(t) = \mathrm{H}^{-1}(x_1(t^i))(\Gamma(x(t^i)) \\ + M(x_1(t^i))\ddot{q}_d(t) - M(x_1(t^i))\frac{\alpha_1 q}{\alpha_2 p}\dot{e}(t^i)^{2-p/q} \\ - (b_0 + b_1 \|x(t^i)\| + \lambda)sign(S(t^i))), \tag{29}$$

where λ is a positive constant. The event-triggering rule is defined as

$$\|E(t)\| \leq k\|e(t)\| + \xi, \tag{30}$$

where k & $\xi \in \mathbb{R}_0$. Consider $\bar{\Delta} := \inf\{\Delta^i | \Delta^i = t^{i+1} - t^i, \ i \in \mathbb{N}_0\}$, $t^0 = 0$, under the event-triggering rule (30), $\bar{\Delta}$ satisfies the following inequality

$$\bar{\Delta} \leq \\ \frac{1}{\|M^{-1}(x_1(t))\| L_0} Ln\left(\frac{\|M^{-1}(x_1(t))\| L_0}{\delta}(k\|e(t)\| + \xi) + 1\right). \tag{31}$$

Proof. Consider the Lyapunov candidate function for the dynamic system (17) as follows

$$V(t) = \frac{0.5}{\beta_\Gamma}S^T(t)S(t), \tag{32}$$

where $\beta_\Gamma = \max(0.5\, S^T(t)S(t))$. Differentiating from (32) with respect to time $t \in [t^i, t^{i+1}), i \in \mathbb{N}_0$ and considering (26) yields

$$\dot{V}(t) = S^T(t)\dot{e}(t)_d^{p/q-1}(\alpha_1\dot{e}(t)^{2-p/q} + \alpha_2\frac{p}{q}\ddot{e}(t)), \tag{33}$$

Let $\mathrm{H}(x_1(t^i)) = \mathrm{H}(x_1(t) + \partial x_1(t))$, then $\mathrm{H}(x_1(t) + \partial x_1(t))$ can be represented as

$$\mathrm{H}(x_1(t) + \partial x_1(t)) = \mathrm{H}(x_1(t)) - \Delta\mathrm{H}, \tag{34}$$

Now, according to the small perturbation theorem, $\mathrm{H}^{-1}(x_1(t))$ can be defined as follows

$$\mathrm{H}^{-1}(x_1(t^i)) = \mathrm{H}^{-1}(x_1(t)) + \{\mathrm{H}^{-1}(x_1(t))\}\Delta\mathrm{H}\{\mathrm{H}^{-1}(x_1(t))\}, \tag{35}$$

where $\Delta\mathrm{H} \in \mathbb{R}^{n \times n}$ is the norm-bounded matrix and satisfies $\|\Delta\mathrm{H}\,\mathrm{H}^{-1}(x_1(t))\| \leq \bar{H}_\Delta$, where $\bar{H}_\Delta < 1$. Let the control input be $u(t) = \mathrm{H}^{-1}(x_1(t^i)) \times u^*(t)$. By substituting the control effort (29) into (33), and considering (35), and Assumption 7, one can obtain

$$\dot{V}(t) = \frac{1}{\beta_\Gamma}S^T(t)\dot{e}(t)_d^{p/q-1}\{\alpha_2\frac{p}{q}M^{-1}(x_1(t))[\Gamma(x(t^i)) \\ - \Gamma(x(t)) - D(x(t)) - (\lambda + b_0 + b_1\|x(t^i)\|)sign(S(t^i)) \\ + \Delta\mathrm{H}\,\mathrm{H}^{-1}(x_1(t))u^*(t)] \\ + \alpha_1(\dot{e}(t)^{2-p/q} - \dot{e}(t^i)^{2-p/q})\}. \tag{36}$$

According to Lemma 1, and Assumption 1, outside the region Ξ, (36) can be expressed as [55]

$$\dot{V}(t) \leq \frac{1}{\beta_\Gamma}\|S^T(t)\|\left\|\dot{e}(t)_d^{p/q-1}\right\|\{\alpha_2\frac{p}{q}\|M(x_1(t))^{-1}\| \\ [(L_0+b_1)\|E(t)\| - \lambda + \bar{H}_\Delta\|u^*(t)\|] \\ + \alpha_1(\left\|\dot{e}(t)^{2-p/q} - \dot{e}(t^i)^{2-p/q}\right\|)\}. \tag{37}$$

Remark 3: According to the dynamic equation (17), and Assumption 1, $u^*(t)$ is bounded and can be represented as

$$\|u^*(t)\| \leq \bar{u} + \lambda, \tag{38}$$

where $\bar{u} = \|\Gamma(x(t))\| + \|M(x_1(t))\ddot{q}_d(t)\| + \left\|M(x_1(t))\frac{\alpha_1 q}{\alpha_2 p}x_d(t)^{2-p/q}\right\| + b_0 + b_1\|x(t^i)\|$.

Recalling (37) and considering Lemma 2, yields

$$\dot{V}(t) \leq \frac{1}{\beta_\Gamma}\|S^T(t)\|\left\|\dot{e}(t)_d^{p/q-1}\right\| \times \\ \{\alpha_2\frac{p}{q}\|M(x_1(t))^{-1}\|[(L_0+b_1)k\|e(t)\| + \\ (L_0+b_1)\xi - (1 - \bar{H}_\Delta)\lambda + \bar{H}_\Delta\bar{u}] + \alpha_1\Pi\}. \tag{39}$$

By letting $\lambda > (1 - \bar{H}_\Delta)^{-1}\{\frac{\alpha_1}{\alpha_2}\frac{q}{p}\bar{M}\Pi + (L_0+b_1)k\|e(t)\| + (L_0 + b_1)\xi + \bar{H}_\Delta\bar{u}\}$, we have

$$\dot{V}(t) \leq -\eta\|V(t)\|^{0.5}, \tag{40}$$

where $\eta = \{\sqrt{\frac{2}{\beta_\Gamma}}\alpha_2\frac{p}{q}\left\|\dot{x}_d^{\frac{p}{q}-1}(t)\right\|\|M(x_1(t))^{-1}\|[(L_0 + b_1)k\|e(t)\| + (L_0+b_1)\xi + (1 - \bar{H}_\Delta)\lambda + \bar{H}_\Delta\bar{u}] + \alpha_1\Pi\}$.

Then, according to (40), the finite-time convergence is achieved under the proposed controller effort (29) [56]. Proof is complete here.

C. Admissibility of event-trigger controller

The aim of this section is to investigate the admissibility of the proposed controller and introduce the Zeno-free behavior of the presented event-based scheme. By considering dynamic equation (17), and the control effort (29), in the time interval $t \in [t^i, t^{i+1}), i \in \mathbb{N}_0$, one can obtain

$$\dot{E}(t) = M^{-1}(x_1(t))\{-\Gamma(x(t)) - D(x(t)) \\ + \mathrm{H}(x_1(t))[\mathrm{H}^{-1}(x_1(t^i))(\Gamma(x(t^i)) \\ + M(x_1(t^i))\ddot{x}_d(t) - M(x_1(t^i))\frac{\alpha_1 q}{\alpha_2 p}\dot{e}(t^i)^{2-p/q} \\ - (b_0 + b_1\|x(t^i)\| + \lambda)\,sign(S(t^i)))]\}. \tag{41}$$

Then, recalling (34) yields

$$\dot{E}(t) = M^{-1}(x_1(t))\{-\Gamma(x(t)) - D(x(t)) \\ + [I + \Delta\mathrm{H}\,\mathrm{H}^{-1}(x_1(t))](\Gamma(x(t^i)) \\ + M(x_1(t^i))\ddot{x}_d(t) - M(x_1(t^i))\frac{\alpha_1 q}{\alpha_2 p}\dot{e}(t^i)^{2-p/q} \\ - (b_0 + b_1\|x(t^i)\| + \lambda)sign(S(t^i)))\}. \tag{42}$$

Recalling that $u(t) = \mathrm{H}^{-1}(x_1(t^i)) \times u^*(t)$, (42) can be rewritten as

$$\dot{E}(t) = M^{-1}(x_1(t))\{\Gamma(x(t^i)) - \Gamma(x(t)) - D(x(t)) \\ - (b_0 + b_1\|x(t^i)\| + \lambda)sign(S(t^i)) \\ + M(x_1(t^i))\ddot{x}_d(t) - M(x_1(t^i))\frac{\alpha_1 q}{\alpha_2 p}\dot{e}(t^i)^{2-p/q} \\ + [\Delta\mathrm{H}\,\mathrm{H}^{-1}(x_1(t))]u^*(t)\}. \tag{43}$$

Considering (18) yields

$$\left\| \dot{E}(t) \right\| \leq \left\| M^{-1}(x_1(t)) \right\| \{ L_0 \left\| E(t) \right\| + 2\bar{D} + \lambda$$
$$+ \left\| M(x_1(t^i)) \ddot{x}_d(t) \right\| + \frac{\alpha_1 q}{\alpha_2 p} \left\| M(x_1(t^i)) \right\| \times$$
$$\left\| \dot{x}_d(t)^{2-p/q} \right\|) + \bar{H}_\Delta \left\| u^*(t) \right\| \},$$

(44)

where $\bar{D}$ is the upper bound of $D(x(t))$, i.e., $\|D(x(t))\| \leq \bar{D}$. Note that due to the stability analysis, proposed in subsection III-B, it is reasonable to consider uncertain terms are bounded due to the boundedness of $x(t)$. Then, by defining

$$\delta = \left\| M^{-1}(x_1(t)) \right\| \left\{ \beta^* + \bar{H}_\Delta \|u^*(t)\| + \lambda \right\}, \quad (45)$$

where
$\beta^* = \{ 2\bar{D} + \|M(x_1(t^i))\| \|\ddot{x}_d(t)\| + \frac{\alpha_1 q}{\alpha_2 p} \|M(x_1(t^i))\| \|\dot{x}_d(t)\|^{2-p/q} \}$.

By solving the ordinary differential equation, and considering $E(t^i) = 0$ as a boundary condition, the inequality (44) can be represented as

$$\|E(t)\| \leq \frac{\delta}{\|M^{-1}(x_1(t))\| L_0} * (e^{\|M^{-1}(x_1(t))\| L_0 \Delta} - 1). \quad (46)$$

Then, by considering (30) one can obtain (31).

Remark 4: By considering Assumption 4, the parameters δ, and ξ, the right-hand side of the inequality (31) is always greater than zero. Then, the Zeno-free behavior of the proposed method is guaranteed.

D. Cyber attack investigation

In subsection III-B, the stability analysis in the presence of event-based controller is investigated. It was proven that if the states are updated in a way that the inequality (30) holds, the finite-time convergence is achieved according to (40). Now, in this section the situation where the inequality (30) does not hold due to the cyber-attack is investigated [54]. The inequality (37) can be rewritten as

$$\dot{V}(t) \leq \gamma_1 \|E(t)\| - \gamma_2 V(t)^{0.5}, \quad (47)$$

where $\gamma_1 = \frac{1}{\beta_\Gamma} \|S^T(t)\| \left\| \dot{e}(t)_d^{p/q-1} \right\| \{ \alpha_2 \frac{p}{q} \|M^{-1}(x_1(t))\| \times (b_1 + L_0) \}$, and $\gamma_2 = \frac{1}{\beta_\Gamma} \|S^T(t)\| \left\| \dot{e}(t)_d^{p/q-1} \right\| \times \{ \alpha_2 \frac{p}{q} \|M^{-1}(x_1(t))\| [\lambda - \bar{H}_\Delta \|u^*(t)\|] - \varpi \}$, where $\varpi = \alpha_1 (\left\| \dot{e}(t)^{2-p/q} - \dot{e}(t^i)^{2-p/q} \right\|)$. Now, by considering $\|V(t)\| \leq 1$, (47) can be rewritten as:

$$\dot{V}(t) \leq \gamma_1 \|E(t)\| - \gamma_2 V(t). \quad (48)$$

Expressing (48) in time-domain yields

$$V(t) \leq \frac{\gamma_1}{\gamma_2} \|E(t)\| + e^{-\gamma_2 t} V(0). \quad (49)$$

In this step, time vector is divided into two separate groups. One of them represents time-instances in which (30) holds, i.e., $\widehat{\mathbb{Q}}$, and its compliment defines duration in which (30) does not hold, i.e., $\mathbb{Q}$ as follows

$$\mathbb{Q} := \{ \bigcup_{i \in N_0} [t_i, t_i + \psi_i] \}. \quad (50)$$

Note that $t_0 = \psi_0 = 0$. For any $t \in \widehat{\mathbb{Q}}$, $V(t)$ can be expressed as

$$V(t) \leq V(t_i + \psi_i) e^{-\eta(t-(t_i+\psi_i))}. \quad (51)$$

Then, in $t \in \mathbb{Q}$, by considering (49), $V(t)$ can be calculated as

$$V(t) \leq \frac{\gamma_1}{\gamma_2} \|E(t)\| + e^{-\gamma_2(t-t_i)} V(t_i). \quad (52)$$

Now, $Q(\tau, t)$ and $\widehat{Q}(\tau, t)$ are defined as follows

$$Q(\tau, t) = [\tau, t) \bigcap \mathbb{Q}, \quad (53)$$

and

$$\widehat{Q}(\tau, t) = [\tau, t) \bigcap \widehat{\mathbb{Q}}, \quad (54)$$

where $t > \tau$, and $\mathbb{Q}$ represents the checkerboard areas in Fig. 3. Now, by considering (51), (52), (53), and (54), $V(t)$ can be defined as

$$V(t) \leq e^{-\eta\{\widehat{Q}(0,t)\} - \gamma_2\{Q(0,t)\}} +$$
$$\frac{\gamma_1}{\gamma_2} \|E(t)\| (1 + \sum_{\substack{i \in N_2 \\ t > t_i}} e^{-\eta\{\widehat{Q}(t_i,t)\} - \gamma_2\{Q(t_i,t)\}}).$$

(55)

By considering $\widehat{Q}(0,t) = t - Q(0,t)$, one can obtain

$$-\eta \left\{ \widehat{Q}(t_i,t) \right\} - \gamma_2 \left\{ Q(t_i,t) \right\} = (\eta - \gamma_2) \left\{ Q(t_i,t) \right\} - \eta(t-t_i). \quad (56)$$

According to Assumption 1, $\Gamma(x(t))$ is Lipchitz on the compact set $\Omega \in \mathbb{R}^n$, and one can obtain $\ell \in \mathbb{R}_0$ such that $\|\Gamma(x(t))\| \leq \ell \|x(t)\|$ [57]. Then,

$$\|E(t)\| \leq \left\{ \|x(t_i)\| (1 + b_1) + \frac{1}{\ell} + b_0 \right\} \times$$
$$\left\{ e^{\ell \left\{ (n_0 + \frac{t-t_i}{\tau_0})(d_0 + \frac{t-t_i}{\nu}) + (1+n)\bar{\Delta} \right\}} + 1 \right\}$$

(57)

Now, by considering (55) and (56), the stability is preserved if the following constraint is satisfied

$$\ell\{(n)Q(t_i,t) + (1+n)\bar{\Delta}\} + (\eta - \gamma_2) \{Q(t_i,t)\} - \eta\bar{\Delta} < 0. \quad (58)$$

Finally, the proposed scheme shows a resilient behavior as long as the following inequality holds,

$$Q(t_i,t) < \frac{\bar{\Delta}\{-(1+n)\ell + \eta\}}{\{\ell n + (\eta - \gamma_2)\}}. \quad (59)$$

Remark 5: The designed methodology is based on the passive resilient control type and can be extended to the false data injection (FDI) type of cyber-attacks. Note that to cover other type of malicious attack needs to utilized active resilient methodology by utilizing compromised-data estimators.

IV. SIMULATION RESULTS

In this section, the proposed control scheme is validated through an experimental simulation on the verified model of the Brokk- Hydrolek 7-DoF manipulator, illustrated in Fig. 1.

The parameters estimated for the manipulator model are based on several experimental works carried out on the robot. For a detailed explanation of the experimental

Parameter	Description	Value
$[m_1, m_2]$	mass of the links	$[4, 22.2]\, kg$
$[A_a, A_b]$	piston areas	$[0.0015, 0.001]\, m^2$
$[l_{base1}, l_{base2}]$	length of base	$[0.317, 0.1]\, m$
$[l_{link1}, l_{link2}]$	length of link	$[0.1, 0.1]\, m$
$[P_s, P_t]$	hydraulic pressure	$[180, 0.5]\, bar$
k_p	pressure-flow coefficient	$[0.0023, 0.0041]$
k_{q_a}	flow gain	$10^5[3.4225, 3.5968]$
k_{q_b}	flow gain	$10^5[3.4296, 2.4871]$
x_{c_1}, x_{c_2}	link's center of mass position in x axis	$[0.09, 0.5116]$
d_2	DH parameters of robot	0.0032
a_1	DH parameters of robot	0.1273
I_{minA}	low limit of electrical current: solenoid A	$[0.0703, 0.0718]A$
I_{minB}	low limit of electrical current: solenoid B	$[0.0751, 0.0710]A$

study and the method proposed to estimate the manipulator parameters an interested reader is referred to several previous attempts reported in [9]-[48]. As can be inferred from the experimental results in [9], the coupling effect between the links is significant for two consecutive links. Therefore, for the control purpose it would be reasonable to assume that the system dynamic consists of a 2-DoF model for the manipulator and the effect of other links and joints is considered as the uncertainty in the lumped generalised disturbance term in the subsequent analysis. In this case, the mass matrix $M(q) \in \mathbb{R}^{2\times2}$ in (17) as the state-space model of the manipulator can be written as

$$M(q) = \begin{bmatrix} M_1 & M_2 \\ M_3 & M_4 \end{bmatrix}, \qquad (60)$$

where $M_1 = m_1 x_{c_1}^2 + a_1 m_1 \cos(q_2) x_{c_2} + m_2 \cos(q_2)^2 x_{c_2}^2$, $M_2 = -d_2 m_2 \sin(q_2) x_{c_2}$, $M_3 = M_2$, and $M_4 = m_2 x_{c_2}^2$. The parameters estimated for the manipulator, including the mechanical, electrical, and hydraulic constants are listed in Tables I. Moreover, the gravity torque vector is defined as $G(q) = \begin{bmatrix} 0 & m_2 x_{c_2} \cos(q_2) g \end{bmatrix}^T$, where $g = 9.81 \frac{m}{s^2}$, and

$$C(q, \dot{q}) = \begin{bmatrix} C_1 & C_2 \\ C_3 & C_4 \end{bmatrix}, \qquad (61)$$

where

$C_1 = (a_1^2 m_2 + m_2 d_2^2 + cos(q_2) m_2 x_{c_2} a_1) - (m_2 sin(q_2) x_{c_2} (cos(q_2) x_{c_2} + a_1) \dot{q}_2)$, $C_2 = (-d_2 cos(q_2) m_2 x_{c_2} \dot{q}_2)$, $C_3 = (m_2 x_{c_2} sin(q_2)((a_1 + +x_{c_2} sin(q_2)) \dot{q}_1 - d_2))$, and $C_4 = 0$. Finally, $F(\dot{q}) = 40[\ \dot{q}_1 \quad \dot{q}_2\ ]^T$.

The controller design parameters are chosen as $p = 5$, $q = 3$, $k = 0.001$, $\xi = 0.001$, $\alpha_1 = 0.1$, $\alpha_2 = 0.7$, $\lambda = 40$ and $D = 0.01[sin(q_1), sin(q_2)]^T$. The parameters p, q, α_1, and α_2 specify the dynamic of the sliding surface, and can be determined based on the desired states responses. Note that inequality $1 < \frac{p}{q} < 2$ should be satisfied to avoid the singularity in the control effort. The parameters k and ξ define the event-triggering rule according to (30). Although increasing the values of these constants yields decreasing the number of transmitted data packets toward the controller, it increases the steady-state error. Note that violating inequality (39) would destabilize the closed-loop control system.

Remark 6: To overcome the chattering issue, an alternative smooth function, i.e., $tanh$, is utilized in the simulations instead of the $signum$ function.

Test id	1	2	3	4
DoS attack duration	10%	20%	30%	40%

The stabilized response of the robotic manipulator in presence of DoS attacks is depicted in Fig. 4(a). It is assumed that the attack frequency is 1Hz and 10% of measurement data is ruined by the attackers in each period. As illustrated in this figure, a proper regulation around the desired set-point is achieved by overcoming the effect of cyber-attacks. To consider the experimental conditions, a white noise with the variance value 2.5×10^{-6}, and the mean value -1.5×10^{-5}, added for measurement of the system states, i.e., q and $\dot{q}$. Closed-loop responses under the same designed parameters and cyber-attacks are depicted in Fig.4(c).

In Fig. 4(b), and 4(d) the inter-sampling time evolution is shown in the absence, and presence of the noise respectively. As illustrated in this figure, the minimum inter-sampling time occurs exactly when the tracking error passes its maximum deviation rate. This is a sensible result following the inequality (30). Decreasing the deviation rate of the tracking error results in a decrease in the deviation rate of the event-triggering error. As can be seen in Fig. 4(b), this happens by increasing the inter-sampling time intervals. On the other hand, after passing the transient time, the inter-sampling time increases because there is no triggering error $E(t)$. In this phase, ξ plays an important role. Although the increase in ξ yields a higher inter-sampling time and transmission of less data, it has a side effect on the response behavior of the controller and increases the steady-state tracking error of the response. Therefore, the Zeno-free behavior of the controller is validated in Fig. 4 in this way.

As illustrated in Fig 4.(d), due to the white noise signal deviation rate, inter-sampling time decreases compared to the noise-free responses. Fig. 5 demonstrates the event-triggered transmitted-states. As shown in this figure, the number of event-triggering rule activation decreases after passing the transient phase. The sliding surface dynamic for each joint and the effect of cyber-attack, and measurement noise on the evolution of these surfaces are shown in Fig. 6.

To evaluate the resilience behavior of the proposed approach, four tests are carried out as listed in Table II. The mean and variance values of the tracking error in each case are plotted in Fig. 7. As shown in this figure, the closed-loop stability is preserved even while 40% of transmitted data are ruined by adversaries. Note that the number of transmitted data packets under the proposed event-based TSMC (ETSMC) is 7825, and the number of transmitted data packets under the TSMC is 30001 while the simulation time in both tests is 10 sec. Although the number of transmitted data packets may vary in different tests, reported data proves the effectiveness of the proposed ETSMC in communication usage reduction.

To show the effectiveness of the proposed method in tracking tasks, simulations are
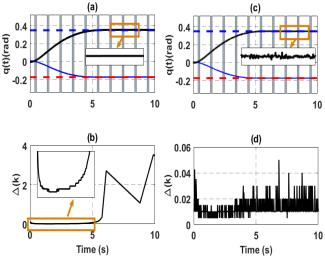
Fig. 4. (a) and (c) show the joint angles' trajectories, $q_1(t)$ and $q_2(t)$, under the proposed approach in the absence, and presence of measurement noise respectively. The blue, and black solid lines demonstrate $q_1(t)$ and $q_2(t)$ respectively. The horizontal dashed-lines defines the desired states Note that in both simulation scenarios, DoS attacks ruin 10% of the transmitted data, as shown by the solid vertical lines. The desired states are $[-10, 20]deg$ equal to $[-0.1745, 0.3491]rad$. (b), and (d) demonstrate inter-sampling time evolution regarding the (a), and (c) states' evolution, respectively.

Fig. 5. Event-triggered transmission data in the absence of measurement noise.

performed by considering desired trajectories $q_{des} = 0.035 * [\sin(0.3t), \sin(0.3t)]rad$. As shown in Fig. 8, the proposed TSMC, and ETSMC demonstrate satisfying responses. The ultimate bounded response of tracking error is verified through Fig. 8.c, and Fig. 8.d. according to the Lemma 1.

As stated in Section I, proposing an efficient criterion to evaluate the performance of EHRMs is always a challenging issue. ρ index is a feasible way to show the effectiveness of different control schemes for robotic manipulators, that is defined as follows [18], [25], [58]:

$$\rho = \frac{\max(|x - x_{des}|)}{\max(|\dot{x}|)} = \frac{|e|_{max}}{|\dot{x}|_{max}} \quad (62)$$

The smaller the ρ, shows the better performance of the concerned control scheme. In Table III, non-singular TSMC, and ETSMC that are proposed in this study are compared with some prior studies including event-based, and non-event-based approaches that are presented for the control tasks of robot manipulators. As stated in this table, TSMC shows the best performance according to the reported ρ index. The index $\sigma \in (0, 1]$ demonstrates the ratio between the number of requests to transmit data packets, and the number of transmission executions. Obviously in nonevent-based structures $\sigma = 1$. Then, the smaller the σ, shows the lower communication resources usage, lower controller's input updates, the higher optimality in the network layer, and the higher energy saving efficiency. Note that increasing the value ξ, yields to decrease σ, and increase ρ. Then, there is a trade-off between σ, and ρ
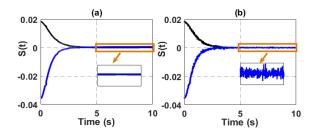

Fig. 6. The time evolution of sliding surface dynamic for each joint: (a) in the absence of noise; (b) in the presence of noise.
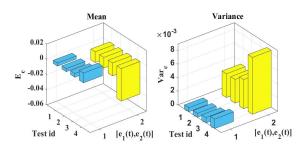

Fig. 7. Mean, and variance values of tracking error for the four tests that are carried out according to Table II. Graphs with blue and yellow colors relate to first and second joints respectively.

to choose ξ, k. In Table III, ETSMC performances based on the two ξ values are reported. As demonstrated in this table, best performance compared with the prior studies, based on the ρ, and σ indexes, is achieved through utilizing the proposed scheme in this study.
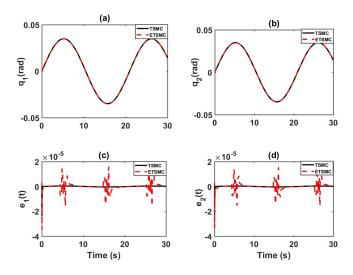

Fig. 8. (a), and (b) show q_1, and q_2 responses under the proposed schemes. (c), and (d) demonstrate q_1, and q_2 tracking errors, respectively.

Remark 7: The proposed method can be extended to the periodic event-based methodology with cycle time h that satisfies inequality $0 < h \leq \bar{\Delta}$.

V. CONCLUSION

In this study, an event-based terminal sliding mode controller is proposed for an uncertain 7-DoF hydraulically actuated robotic manipulators that uses network to transmit data. The dynamic model of the manipulator combined with the hydraulic actuator is derived in a general form

TABLE III
COMPARISON OF ρ, AND σ INDEXES FOR DIFFERENT SCHEMES.

Study	$|e|_{\max}$	$\rho(s)$	σ
Zhu 2005 [58] *	$0.0005 rad$	0.005	1
Bech 2013 [59] **	$2.05 mm$	0.0044	1
Koivumäki 2015 [60] **	$0.61 mm$	0.0030	1
Mustafa 2019 [55]†	$1.6\ rad$	0.5	0.414
Lee 2020 [61]††	$0.08 rad$	0.0030	1
Zhang 2021 [62]†††	$5.5 mm$	0.0275	0.387
TSMC developed in this study	$0.00014 rad$	0.0013	1
ETSMC developed in this study‡	$0.00037 rad$	0.003	0.85
	$0.00049 rad$	0.0181	0.31

* $|e|_{\max}$ is shown in Fig. 19(b), and ρ is reported in Section 4, page 11 of 12, in [58].
** Data are reported in Table I of [18]. Note that, $|e|_{\max}$ represents piston tracking error.
† Data are reported in the Table 1 of study [55].
†† In [61], control performance is reported based on the control gain variation in the domain $K_p = (0.001 - 1)$, then $|e|_{\max}$ is derived from Fig.8(a), and Fig8(c) in [61] that relate to $K_p = 0.001$, and $K_p = 1$, respectively. Note that $|\dot{x}|_{\max}$ is calculated from the sinusoidal desired position.
††† Data are reported in section V. A of study [62].
‡ Increasing the value of ξ yields to increase $\rho(s)$, and decrease σ. First, and second rows report indexes while $\xi = 0.01$, and $\xi = 0.001$, respectively.

and validated experimentally. The proposed methodology guarantees the finite-time stability as well as the robust and resilient behavior in the presence of unknown dynamics and cyber-attacks. An explicit relation between DoS attack properties, i.e., attack duration and frequency, with the controller parameters is derived and the criteria to achieve a resilient performance is expressed. Finally, the effectiveness of the proposed scheme is analyzed through an experimental benchmark. The obtained results confirm the superiority of the proposed approach compared to state-of-the-art schemes based on the ρ index criterion. Future studies can focus on the problem of network delay that affects the response behavior in the practical experiments. Moreover, a dynamic event-triggering scheme can be utilized to decrease the amount of transmitted data while the desired response is preserved.

APPENDIX

Proof of Lemma 1: Recalling the sliding surface dynamic (25), and (26) yield:

$$S(t^i) - S(t) = \alpha_1\{e(t^i) - e(t)\} + \alpha_2\{\dot{e}(t^i)^{p/q} - \dot{e}(t)^{p/q}\}. \quad (63)$$

By considering the event-triggering error (27) and the triggering rule (30), the expression (63) can be rewritten as

$$\left\|S(t^i) - S(t)\right\| \leq \alpha_1\{k\left\|e(t)\right\| + \xi\} \\ + \alpha_2\left\|\dot{x}_d(t)^{p/q} + \frac{e(t)}{\Delta}^{p/q}\right\|. \quad (64)$$

Note that here we are analyzing the switching phase or the time that the sliding surface dynamic has passed the reaching phase. In this situation, $e(t) \approx 0$. Now, assuming that the derivation of $x_d(t)$ in $t \in [t^n, t^{(n+1)})$ can be neglected, the expression in (64) can be simplified to

$$\left\|S(t^n) - S(t)\right\| \leq \alpha_1\xi, \quad (65)$$

where $[t^{n^-}, t^{n^+})$ is the time interval when $sign(S(t))$ changes its sign at $S(t^n)$. Therefore, the region Ξ in which

$Sign(S(t^i)) \neq Sign(S(t))$ will be a closed region. Note that the $\max\{\|S(t)\|\,|\,t \in [t^{n^-}, t^{n^+})\}$ is derived when $S(t^n) = 0$. Then,

$$\max\{\|S(t)\|\,|\,t \in [t^{n^-}, t^{n^+})\} = \alpha_1\xi. \quad (66)$$

The ultimate bound of the state trajectories can be derived by considering sliding surface dynamic (25). Now, consider a Lyapunov candidate function,

$$V_n(t) = 0.5 e^T(t)e(t), \quad (67)$$

where $e(t)$ is tracking error. Then, by finding derivative of $V_n(t)$ along time,a and having (25), one can obtain that the $\dot{V}_n(t)$ is negative definite as long as $\|e(t)\| > \alpha_1^{-1}\|S(t)\|$. Note that calculation is proposed for switching-phase duration. Then, the upper-bound of the $\|e(t)\| > \xi$. This completes the proof.

Proof of Lemma 2: Recalling (27), $e(t)$ can be represented as

$$\dot{e}(t) = \dot{E}(t) - \dot{x}_d(t). \quad (68)$$

From (30) and definition of $\bar{\Delta} := \inf\{\Delta^i|\Delta^i = t^{i+1} - t^i, i \in N_0\}$, $t^0 = 0$, one can obtain

$$\|\dot{e}(t)\| \leq k\frac{\|e(t)\|}{\bar{\Delta}} + \|\dot{x}_d(t)\|. \quad (69)$$

Then, by considering (69) one can obtain

$$\left\|\dot{e}(t)^{2-p/q} - \dot{e}(t^i)^{2-p/q}\right\| \leq \\ \max\{1, (k\frac{\|e(0)\|}{\bar{\Delta}} + \|\dot{x}_d(t)\| + \xi)^{2-p/q} + \|\dot{x}_d(t)\|^{2-p/q}\}. \quad (70)$$

This completes the proof.

REFERENCES

[1] M. Bandala, C. West, S. Monk, A. Montazeri, and C. J. Taylor, "Vision-based assisted tele-operation of a dual-arm hydraulically actuated robot for pipe cutting and grasping in nuclear environments," *Robotics*, vol. 8(2), no. 42, pp. 1–24, 2019.

[2] T. Burrell, A. Montazeri, S. Monk, and C. J. Taylor, "Feedback control—based inverse kinematics solvers for a nuclear decommissioning robot," *IFAC-PapersOnLine*, vol. 49, no. 21, pp. 177–184, 2016.

[3] F. Cursi, W. Bai, E. M. Yeatman, and P. Kormushev, "Optimization of surgical robotic instrument mounting in a macro–micro manipulator setup for improving task execution," *IEEE Transactions on Robotics*, vol. 38, no. 5, pp. 2858 – 2874, 2022.

[4] Y. Huang, Y. S. Yong, R. Chiba, T. Arai, T. Ueyama, and J. Ota, "Kinematic control with singularity avoidance for teaching-playback robot manipulator system," *IEEE Transactions on Automation Science and Engineering*, vol. 13, no. 2, pp. 729–742, 2015.

[5] R. Prakash, L. Behera, S. Mohan, and S. Jagannathan, "Dual-loop optimal control of a robot manipulator and its application in warehouse automation," *IEEE Transactions on Automation Science and Engineering*, 2020.

[6] Q. Guo and D. Jiang, *Nonlinear Control Techniques for Electro-Hydraulic Actuators in Robotics Engineering*. CRC Press, 2017.

[7] J. Lee, P. H. Chang, and M. Jin, "Adaptive integral sliding mode control with time-delay estimation for robot manipulators," *IEEE Transactions on Industrial Electronics*, vol. 64, no. 8, pp. 6796–6804, 2017.

[8] N. Norsahperi and K. Danapalasingam, "An improved optimal integral sliding mode control for uncertain robotic manipulators with reduced tracking error, chattering, and energy consumption," *Mechanical Systems and Signal Processing*, vol. 142, p. 106747, 2020.

[9] A. Montazeri, C. West, S. D. Monk, and C. J. Taylor, "Dynamic modelling and parameter estimation of a hydraulic robot manipulator using a multi-objective genetic algorithm," *International Journal of Control*, vol. 90, no. 4, pp. 661–683, 2017.

[10] S. Lyu and C. C. Cheah, "Data-driven learning for robot control with unknown jacobian," *Automatica*, vol. 120, p. 109120, 2020.

[11] H. Su, Y. Hu, H. R. Karimi, A. Knoll, G. Ferrigno, and E. De Momi, "Improved recurrent neural network-based manipulator control with remote center of motion constraints: Experimental results," *Neural Networks*, vol. 131, pp. 291–299, 2020.

[12] T. Yang, N. Sun, Y. Fang, X. Xin, and H. Chen, "New adaptive control methods for n-link robot manipulators with online gravity compensation: Design and experiments," *IEEE Transactions on Industrial Electronics*, 2021.

[13] E. A. Alandoli and T. S. Lee, "A critical review of control techniques for flexible and rigid link manipulators," *Robotica*, vol. 38, no. 12, pp. 2239–2265, 2020.

[14] V.-T. Ngo and Y.-C. Liu, "Object transportation with force-sensorless control and event-triggered synchronization for networked uncertain manipulators," *IEEE Transactions on Industrial Electronics*, vol. 68, no. 1, pp. 902–912, 2020.

[15] V. Krueger, A. Chazoule, M. Crosby, A. Lasnier, M. R. Pedersen, F. Rovida, L. Nalpantidis, R. Petrick, C. Toscano, and G. Veiga, "A vertical and cyber–physical integration of cognitive robots in manufacturing," *Proceedings of the IEEE*, vol. 104, no. 5, pp. 1114–1127, 2016.

[16] C. Hildebrandt, A. Köcher, C. Küstner, C.-M. López-Enríquez, A. W. Müller, B. Caesar, C. S. Gundlach, and A. Fay, "Ontology building for cyber–physical systems: Application in the manufacturing domain," *IEEE Transactions on Automation Science and Engineering*, vol. 17, no. 3, pp. 1266–1282, 2020.

[17] D. Ding, Q.-L. Han, Y. Xiang, X. Ge, and X.-M. Zhang, "A survey on security control and attack detection for industrial cyber-physical systems," *Neurocomputing*, vol. 275, pp. 1674–1683, 2018.

[18] J. Mattila, J. Koivumäki, D. G. Caldwell, and C. Semini, "A survey on control of hydraulic robotic manipulators with projection to future trends," *IEIE/ASME Transactions on Mechatronics*, vol. 22, no. 2, pp. 669–680, 2017.

[19] N. Nikdel, M. Badamchizadeh, V. Azimirad, and M. A. Nazari, "Fractional-order adaptive backstepping control of robotic manipulators in the presence of model uncertainties and external disturbances," *IEEE Transactions on Industrial Electronics*, vol. 63, no. 10, pp. 6249–6256, 2016.

[20] D. Nicolis, F. Allevi, and P. Rocco, "Operational space model predictive sliding mode control for redundant manipulators," *IEEE Transactions on Robotics*, vol. 36, no. 4, pp. 1348–1355, 2020.

[21] C. Yang, Y. Jiang, W. He, J. Na, Z. Li, and B. Xu, "Adaptive parameter estimation and control design for robot manipulators with finite-time convergence," *IEEE Transactions on Industrial Electronics*, vol. 65, no. 10, pp. 8112–8123, 2018.

[22] Y. Feng, X. Yu, and Z. Man, "Non-singular terminal sliding mode control of rigid manipulators," *Automatica*, vol. 38, no. 12, pp. 2159–2167, 2002.

[23] T. N. Truong, A. T. Vo, and H.-J. Kang, "A backstepping global fast terminal sliding mode control for trajectory tracking control of industrial robotic manipulators," *IEEE Access*, vol. 9, pp. 31921–31931, 2021.

[24] L. Jin, S. Li, J. Yu, and J. He, "Robot manipulator control using neural networks: A survey," *Neurocomputing*, vol. 285, pp. 23–34, 2018.

[25] W.-H. Zhu, T. Lamarche, E. Dupuis, D. Jameux, P. Barnard, and G. Liu, "Precision control of modular robot manipulators: The vdc approach with embedded fpga," *IEEE Transactions on Robotics*, vol. 29, no. 5, pp. 1162–1179, 2013.

[26] W. Deng, J. Yao, Y. Wang, X. Yang, and J. Chen, "Output feedback backstepping control of hydraulic actuators with valve dynamics compensation," *Mechanical Systems and Signal Processing*, vol. 158, p. 107769, 2021.

[27] R. Ma, P. Shi, and L. Wu, "Dissipativity-based sliding-mode control of cyber-physical systems under denial-of-service attacks," *IEEE Transactions on Cybernetics*, vol. 51, pp. 2306 – 2318, 2020.

[28] D. Li, N. Gebraeel, and K. Paynabar, "Detection and differentiation of replay attack and equipment faults in scada systems," *IEEE Transactions on Automation Science and Engineering*, vol. 18, no. 4, pp. 1626–1639, 2020.

[29] V. Narayanan, S. Jagannathan, and K. Ramkumar, "Event-sampled output feedback control of robot manipulators using neural networks," *IEEE transactions on neural networks and learning systems*, vol. 30, no. 6, pp. 1651–1658, 2018.

[30] E. Kang, H. Qiao, Z. Chen, and J. Gao, "Tracking of uncertain robotic manipulators using event-triggered model predictive control with learning terminal cost," *IEEE Transactions on Automation Science and Engineering*, 2022.

[31] T. Liu, P. Zhang, and Z.-P. Jiang, *Robust Event-Triggered Control of Nonlinear Systems*. Springer, 2020.

[32] Y.-C. Sun and G.-H. Yang, "Periodic event-triggered resilient control for cyber-physical systems under denial-of-service attacks," *Journal of the Franklin Institute*, vol. 355, no. 13, pp. 5613–5631, 2018.

[33] X. Huang, D. Zhai, and J. Dong, "Adaptive integral sliding-mode control strategy of data-driven cyber-physical systems against a class of actuator attacks," *IET Control Theory & Applications*, vol. 12, no. 10, pp. 1440–1447, 2018.

[34] L. An and G.-H. Yang, "Decentralized adaptive fuzzy secure control for nonlinear uncertain interconnected systems against intermittent dos attacks," *IEEE Transactions on Cybernetics*, vol. 49, no. 3, pp. 827–838, 2018.

[35] H. Zhao, Y. Niu, and J. Zhao, "Event-triggered sliding mode control of uncertain switched systems under denial-of-service attacks," *Journal of the Franklin Institute*, vol. 356, no. 18, pp. 11414–11433, 2019.

[36] A. Abbaspour, A. Sargolzaei, P. Forouzannezhad, K. K. Yen, and A. I. Sarwat, "Resilient control design for load frequency control system under false data injection attacks," *IEEE Transactions on Industrial Electronics*, vol. 67, no. 9, pp. 7951–7962, 2019.

[37] Y.-C. Sun and G.-H. Yang, "Periodic event-triggered resilient control for cyber-physical systems under denial-of-service attacks," *Journal of the Franklin Institute*, vol. 355, no. 13, pp. 5613–5631, 2018.

[38] Y. Jiang, S. Wu, H. Yang, H. Luo, Z. Chen, S. Yin, and O. Kaynak, "Secure data transmission and trustworthiness judgement approaches against cyber-physical attacks in an integrated data-driven framework," *IEEE Transactions on Systems, Man, and Cybernetics: Systems*, vol. 52, no. 12, pp. 7799–7809, 2022.

[39] C. Fang, Y. Qi, P. Cheng, and W. X. Zheng, "Optimal periodic watermarking schedule for replay attack detection in cyber–physical systems," *Automatica*, vol. 112, p. 108698, 2020.

[40] Y. Mo, S. Weerakkody, and B. Sinopoli, "Physical authentication of control systems: Designing watermarked control inputs to detect counterfeit sensor outputs," *IEEE Control Systems Magazine*, vol. 35, no. 1, pp. 93–109, 2015.

[41] Y. Wang, C. Lin, Q.-L. Li, and Y. Fang, "A queueing analysis for the denial of service (dos) attacks in computer networks," *Computer Networks*, vol. 51, no. 12, pp. 3564–3573, 2007.

[42] X.-M. Zhang, Q.-L. Han, X. Ge, and L. Ding, "Resilient control design based on a sampled-data model for a class of networked control systems under denial-of-service attacks," *IEEE Transactions on Cybernetics*, vol. 50, no. 8, pp. 3616–3626, 2019.

[43] C. De Persis and P. Tesi, "Input-to-state stabilizing control under denial-of-service," *IEEE Transactions on Automatic Control*, vol. 60, no. 11, pp. 2930–2944, 2015.

[44] S. Hu, P. Yuan, D. Yue, C. Dou, Z. Cheng, and Y. Zhang, "Attack-resilient event-triggered controller design of dc microgrids under dos attacks," *IEEE Transactions on Circuits and Systems I: Regular Papers*, 2019.

[45] A. Montazeri and J. Ekotuyo, "Development of dynamic model of a 7DoF hydraulically actuated tele-operated robot for decommissioning applications," in *2016 American Control Conference (ACC)*, ACC 2016, pp. 1209–1214, IEEE, IEEE, 2016.

[46] C. West, A. Montazeri, S. D. Monk, D. Duda, and C. J. Taylor, "A new approach to improve the parameter estimation accuracy in robotic manipulators using a multi-objective output error identification technique," in *2017 26th IEEE International Symposium on Robot and Human Interactive Communication (RO-MAN)*, pp. 1406–1411, IEEE, IEEE, 2017.

[47] C. West, A. Montazeri, S. D. Monk, and C. J. Taylor, "A genetic algorithm approach for parameter optimization of a 7DoF robotic manipulator," vol. 49, pp. 1261–1266, 2016.

[48] C. West, E. D. Wilson, Q. Clairon, S. D. Monk, A. Montazeri, and C. J. Taylor, "State-dependent parameter model identification for inverse dead-zone control of a hydraulic manipulator," vol. 51, pp. 126–131, 2018.

[49] C. Fallaha, M. Saad, J. Ghommam, and Y. Kali, "Sliding mode control with model-based switching functions applied on a 7-DoF exoskeleton arm," *IEEE/ASME Transactions on Mechatronics*, 2020.

[50] B. Xiao, L. Cao, S. Xu, and L. Liu, "Robust tracking control of robot manipulators with actuator faults and joint velocity measurement uncertainty," *IEEE/ASME Transactions on Mechatronics*, vol. 25, no. 3, pp. 1354–1365, 2020.

[51] J. Song, Y.-K. Wang, Y. Niu, H.-K. Lam, S. He, and H. Liu, "Periodic event-triggered terminal sliding mode speed control for networked pmsm system: A ga-optimized extended state observer

approach," *IEEE/ASME Transactions on Mechatronics*, vol. 27, no. 5, pp. 4153–4164, 2022.

[52] J. Song, Y.-K. Wang, W. X. Zheng, and Y. Niu, "Adaptive terminal sliding mode speed regulation for pmsm under neural-network-based disturbance estimation: A dynamic-event-triggered approach," *IEEE Transactions on Industrial Electronics*, 2022.

[53] J. Song, Y.-K. Wang, and Y. Niu, "Dynamic event-triggered terminal sliding mode control under binary encoding: Analysis and experimental validation," *IEEE Transactions on Circuits and Systems I: Regular Papers*, vol. 69, no. 9, pp. 3772–3782, 2022.

[54] M. Saeedi, J. Zarei, R. Razavi-Far, and M. Saif, "Event-triggered adaptive optimal fast terminal sliding mode control under denial-of-service attacks," *IEEE Systems Journal*, 2021.

[55] A. Mustafa, N. K. Dhar, and N. K. Verma, "Event-triggered sliding mode control for trajectory tracking of nonlinear systems," *IEEE/CAA Journal of Automatica Sinica*, vol. 7, no. 1, pp. 307–314, 2019.

[56] X. Yu and M. Zhihong, "Fast terminal sliding-mode control design for nonlinear dynamical systems," *IEEE Transactions on Circuits and Systems I: Fundamental Theory and Applications*, vol. 49, no. 2, pp. 261–264, 2002.

[57] Y. Yan, S. Yu, and C. Sun, "Quantization-based event-triggered sliding mode tracking control of mechanical systems," *Information Sciences*, vol. 523, pp. 296–306, 2020.

[58] W.-H. Zhu and J.-C. Piedboeuf, "Adaptive output force tracking control of hydraulic cylinders with applications to robot manipulators," 2005.

[59] M. M. Bech, T. O. Andersen, H. C. Pedersen, and L. Schmidt, "Experimental evaluation of control strategies for hydraulic servo robot," in *2013 IEEE International Conference on Mechatronics and Automation*, pp. 342–347, IEEE.

[60] J. Koivumäki and J. Mattila, "High performance nonlinear motion/force controller design for redundant hydraulic construction crane automation," *Automation in construction*, vol. 51, pp. 59–77, 2015.

[61] W. Lee, S. Yoo, S. Nam, K. Kim, and W. K. Chung, "Passivity-based robust compliance control of electro-hydraulic robot manipulators with joint angle limit," *IEEE Robotics and Automation Letters*, vol. 5, no. 2, pp. 3190–3197, 2020.

[62] J. Zhang, L. Jin, and C. Yang, "Distributed cooperative kinematic control of multiple robotic manipulators with improved communication efficiency," *IEEE/ASME Transactions on Mechatronics*, DOI: 10.1109/TMECH.2021.3130592, 2021.